Available online at www.sciencedirect.com
SCIENCE DIRECT®
Journal of Sound and Vibration 290 (2006) 928–955
JOURNAL OF SOUND AND VIBRATION
www.elsevier.com/locate/jsvi

A robust diagnostic model for gearboxes subject to vibration monitoring

Yimin Zhan, Viliam Makis*

Department of Mechanical and Industrial Engineering, University of Toronto, 5 King's College Road, Toronto, Ontario, Canada M5S 3G8

Received 29 July 2003; received in revised form 29 March 2005; accepted 29 April 2005
Available online 1 August 2005

Abstract

This paper presents a robust model-based technique for the detection and diagnosis of gear faults under varying load conditions using the gear motion residual signal. Since the majority of energy in the healthy state of the gear of interest is concentrated at the meshing fundamental and its harmonics, the gear motion residual signal, obtained by the removal of the regular gear meshing fundamental and its harmonics from the time-synchronous average (TSA) signal, will be much less sensitive to the varying load conditions than the TSA signal. Also, the gear motion residual signal usually shows evidence of faults earlier and more clearly than the TSA signal. Therefore, less load dependence and an earlier indication of incipient faults can be obtained simultaneously. A noise-adaptive Kalman filter-based auto-regressive (AR) model is fitted to the gear motion residual signals in the healthy state of the gear of interest. By the selection of a proper model order which provides a compromised model for the healthy gear under various load conditions with the aid of a specific AR model order selection method proposed in this study, further enhancement in load independence can be obtained in the AR model residuals. Consequently, a robust statistical measure, which takes the percentage of outliers exceeding the three standard deviation limits of the baseline AR model residuals, is applied to evaluate the state of the gear of interest. The proposed diagnostic model is validated using full lifetime vibration signals of gearbox operating from new to breakdown under a variety of failure modes and demonstrates remarkable advantages over other newly proposed techniques.

*Corresponding author. Tel.: +1 416 978 4184.
E-mail addresses: yimin.zhan@utoronto.ca (Y. Zhan), makis@mie.utoronto.ca (V. Makis).

0022-460X/$ - see front matter © 2005 Elsevier Ltd. All rights reserved.
doi:10.1016/j.jsv.2005.04.018

1. Introduction

Online condition monitoring of gear transmission systems in industry has attracted increasing interest in recent years, due to the need to decrease the downtime on production machinery and to reduce the extent of the secondary damage caused by failures. Concerning time-domain analyses, the technique of the time-synchronous averaging (TSA) providing a signal that represents the average meshing vibration of one particular gear over a complete revolution has been widely acknowledged as a powerful tool in the detection and diagnosis of gear faults [1–3]. By means of this technique, one can effectively remove any periodic events not exactly synchronous with the gear of interest and reduce the effects of background noise and vibration sources other than the gear of interest. Another appealing processing technique is the extraction of the residual signal by removing the regular gear meshing harmonics from the TSA signal, resulting in a signal predominantly containing the portion that is caused by the gear fault and geometrical irregularity. Apparently the residual signal possesses broadband features due to the abrupt changes caused by localized gear faults and is more desirable for the early detection of gear faults [2]. Currently, most gear fault diagnostic techniques are based upon the gear motion residual signal [4–7]. The pioneering research that proposed the use of the residual signal and the amplitude and phase wavelet maps for the detection of gear faults can be found in Ref. [7].

In general, there are two classes of model-based approaches for condition monitoring of rotating machinery available in the literature: (1) approaches based on parametric modeling such as the one presented in this paper, and (2) flexible models using neural networks and fuzzy logics.

Samanta [8] investigated three types of artificial neural networks (ANNs): a multi-layer perceptron (MLP), radial basis function network (RBF) and probabilistic neural network (PNN), and applied genetic algorithm (GA) for the fault detection of a two-stage gear reduction unit. However, it was pointed out that the retraining of the ANN-based approaches may be required for a changed machine condition with different load.

Other contribution to this area include the papers by Chen and Wang [9], Staszewski et al. [6], Paya et al. [10], Yang et al. [11], Mechefske [12], and Yen and Lin [13], among others.

For implementation of online condition monitoring techniques in practice, a single online state indicator describing the physical condition of the gear of interest is most desirable to compress the huge amount of vibration data and thus present a convenient means of trending the development of gear condition [4]. Statistical measures of the residual signal, which include the root mean square (RMS), change in the RMS (delta RMS), kurtosis [7,14], beta kurtosis [3], etc., are frequently used for this purpose.

Generally speaking, a desirable online state parameter should predominantly satisfy the four conditions: (1) being independent of the variation of load conditions; (2) being able to generate as early as possible an alarm for an incipient fault; (3) indicating a correct description of the severity of a fault state; (4) having low computational requirements.

Conventional vibration monitoring techniques are based on the assumption that changes in the measured signals are caused by deterioration in the condition of the gearbox. However, this assumption is not valid under varying load conditions which are frequently encountered in the practical operation of rotating machinery. Consequently, to find a methodology to deal with varying load conditions is of considerable practical value.

There have been attempts in the recent research to develop a robust method satisfying some of the four conditions. Stander et al. [15] considered various fault and load conditions and found that the Mahalanobis distance could be used as a single parameter to indicate the progression of a fault condition under fluctuating load conditions. However, this method was validated using limited data picked up at a few specific inspections. The stability and effectiveness of this method over the full lifetime horizon has not been investigated. However, such stability is a vital necessity for online condition monitoring since instability of a state index may result in frequent false alarms and at the same time blur the real indication of the incipient faults.

Roan et al. [16] proposed a single state parameter based on an information maximization-based blind source separation algorithm which is able to find the localized damage of the gear of interest. The authors stated that the approach is independent of load conditions. However, such a state parameter cannot be employed by online maintenance decision models since it only illustrates in two-dimensional learning curve plots the severity of the damaged region in comparison with the remaining sound part within one entire revolution of the gear of interest but does not provide a quantitative generalization index of the severity of the fault condition at each inspection.

Baydar and Ball [17] showed that the instantaneous power spectrum can be used to detect local gear faults under different nominal load conditions. This method is based on visual inspection of time–frequency maps and thus a single state parameter can hardly be extracted.

The method developed by Parker et al. [18] possesses a remarkable advantage over the preceding work in that it is independent of load conditions since bicoherence is insensitive to load conditions. However, this method suffers from extensive computational requirements.

Alternative parametric modeling for online vibration monitoring can be established using time-series techniques. An initial study addressing the time-series model-based state diagnostic technique of a gearbox is found in Rantala and Suoranta [19] who proposed a technique which examines the autoregressive (AR) model residuals. However, many key issues were left unsolved in their study, in particular the development and performance analysis of the robust state index under varying load conditions.

Advances in developing an AR model-based state diagnostic model for gearbox were made by Wang and Wong [14] who also proposed a stationary AR model-based diagnostic approach which is to some extent capable of detecting a gear tooth crack earlier than with conventional gear motion residual kurtosis. However, this approach is still load-dependent and the applied state index kurtosis is not reliable as mentioned before and will be further demonstrated in this study.

Our previous study [20] proposed an adaptive parametric model which is transformed from the time-varying AR model and estimated by a noise-adaptive Kalman filter (NAKF). By associating this model with a bispectral domain deterioration detection statistic of a gear, a robust diagnostic technique, which is insensitive to the alternating of load conditions yet capable of quickly indicating the occurrence of gear faults under varying load conditions, is proposed. However, this method is computationally intensive and thus some simplifications must be performed in advance in order to reduce the computational requirements.

In this paper, an efficient diagnostic technique will be proposed which consists of fitting an AR model to gear motion residual signals and then takes advantage of the NAKF to decorrelate the signal to produce a white Gaussian sequence (or AR model residuals). A statistical measure is then applied to the AR model residuals to indicate the state of the gear of interest. The paper

is organized as follows. Section 2 presents the description of the proposed diagnostic model. Section 3 presents the experimental setup. Section 4 presents a comprehensive experimental validation of the proposed method using full lifetime vibration data of a gearbox under various fault conditions. Conclusions are drawn in Section 5.

2. Model description

2.1. Theoretical background

This development is motivated by recognition that the gear motion residual signal represents the departures of the TSA from the average tooth-meshing vibration and usually shows evidence of faults earlier and more clearly than the TSA signal. Thus, fault-induced non-stationary features will be more significant in the gear motion residual signal, whereas the gear motion residual signal is usually stationary in the healthy state of the gear of interest. Most importantly, since much of the energy in the healthy state of the gear of interest is concentrated at the meshing fundamental and its harmonics, the gear motion residual signal, obtained by the removal of the regular gear meshing fundamental and its harmonics from the TSA signal, will be much less sensitive to varying load conditions than the TSA signal. Therefore, earlier alarms for incipient faults and less load dependence can be obtained simultaneously. This corroborates well with the requirements (1) and (2) stated in Section 1.

Further, an NAKF-based AR model is fitted to the stationary gear motion residual signal which corresponds to the initial healthy state of the gear of interest. The resulting AR model coefficients will enable the model to give a consistent prediction for future stationary gear motion residual signals of the same family but yield significant prediction errors for any part that is outside such as fault-induced non-stationarity or any frequency component not contained in the healthy state gear motion residual signal. Therefore, if the gear of interest remains in a healthy state, its model residuals will only represent the prediction error. However, if a localized fault is present, the prediction error will be more significant when the AR model established in the healthy state of the gear of interest is applied.

Most importantly, by the selection of a proper model order for the healthy gear under various load conditions, further enhancement in load-independence can be obtained in the AR model residuals. Consequently, a robust statistical measure termed the model residuals-based machine state deterioration parameter (MRP), which takes the percentage of outliers exceeding the baseline three standard deviation limits can be applied to the AR model residuals to evaluate the state of the gear of interest.

Fig. 1 illustrates in detail the diagram of the proposed model. The model order is determined by selecting a number of gear motion residual signals from the initial period of each load condition under the healthy state of the gear of interest. During the examination of each AR model order candidate, a matrix of state (or time-varying AR model coefficients) vectors with each column corresponding to each angular position (or phase) over the entire revolution of the gear of interest will be obtained by applying the NAKF to the gear motion residual signal at the first inspection. Since the phase information is unavailable in the tests, the mean state vector of this state matrix should be calculated over angular horizon and used as a constant state vector to calculate AR

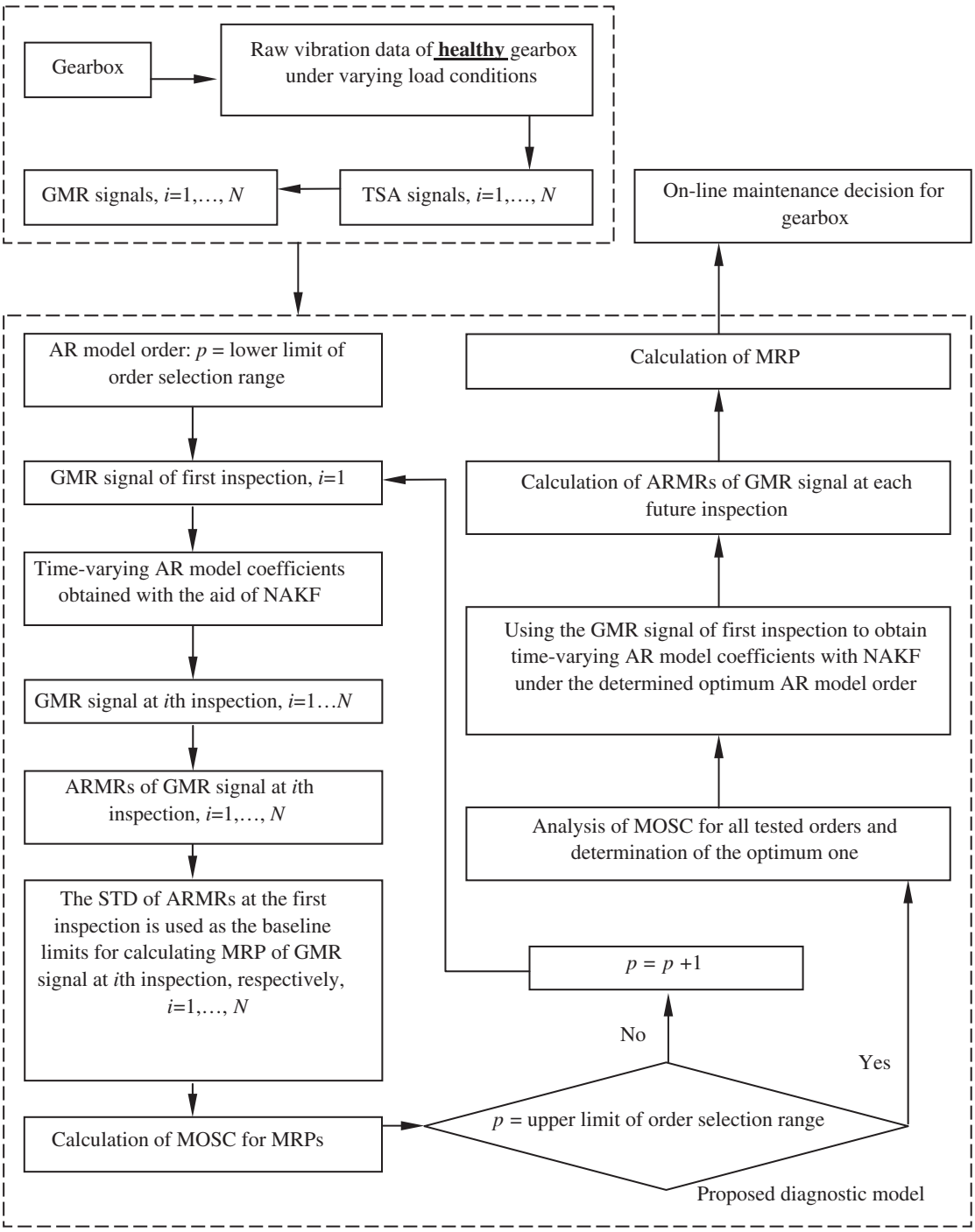

Fig. 1. Diagram of the proposed diagnostic model. Notations: TSA, time synchronous averaging; AR, autoregressive; GMR, gear motion residual; NAKF, noise-adaptive Kalman filter; ARMRs, AR model residuals; STD, standard deviation; MRP, AR model residuals-based gear state parameter; MOSC, model order selection criteria.

model residuals throughout the entire revolution for every inspection performed during the full lifetime of the gear of interest. By doing so, the phase information embedded in the state matrix is lost. This usually would not invalidate the following analysis since the difference among the columns of the state matrix estimated by using the healthy gear's motion residual signals is predominantly induced by the geometric irregularities of the gear of interest which is usually much less significant than fault-induced effects.

The NAKF-based time-varying AR model will be presented in Section 2.2. A novel analytical procedure will be proposed in Section 2.3 to provide a fairly reliable and convenient approach for selecting the optimum AR model order.

2.2. Noise-adaptive Kalman filter

In this section, we present a state-space model transformed from the AR model with time-dependent coefficients, and provide recursive algorithms for the implementation of the Kalman filter. An AR process is a discrete-time multivariate linear stochastic process given by

$$y_i = \sum_{k=1}^{p} A_k y_{i-k} + \varepsilon_i \tag{1}$$

for $i = 1, 2, \ldots, N$, that is, the time series can be considered as the output of a linear all-poles filter driven by a white-noise signal with a flat spectrum, where N is the sample size, p the order of AR model, y_i the ith measurement vector of dimension $d \times 1$, A_k the kth $d \times d$ coefficient matrix of the measurement y_{i-k}, and ε_i a $d \times 1$ sequence of zero-mean white Gaussian measurement noise. Considering the non-stationary property of vibration signatures, we assume the coefficient matrices of the above AR model to be time-varying:

$$y_i = \sum_{k=1}^{p} A_k(i) y_{i-k} + \varepsilon_i. \tag{2}$$

To make use of the Kalman filtering algorithm, it is necessary to develop a state-space representation of model (2). This can be achieved by rearranging the elements of the matrices of coefficients in a vector form using the vec-operator, which stacks the columns of a matrix on top of each other from the left to right side. Then, with the following notation,

$$a_i = \mathrm{vec}([A_1(i), A_2(i) \ldots, A_p(i)]^{\mathrm{T}}), \tag{3}$$

$$Y_i = (y_i^{\mathrm{T}}, y_{i-1}^{\mathrm{T}}, \ldots, y_{i-p+1}^{\mathrm{T}}), \tag{4}$$

$$C_i = I_d \otimes Y_i^{\mathrm{T}} \tag{5}$$

an appropriate state-space representation of the AR model with stochastic coefficients can be given by

$$a_{i+1} = f_i(a_i) + v_i, \tag{6}$$

$$y_i = C_{i-1}^{\mathrm{T}} a_i + \varepsilon_i, \tag{7}$$

where a_i is the $pd^2 \times 1$ state vector, ν_i is an $pd^2 \times 1$ sequence of zero-mean white Gaussian state noise, uncorrelated with a_1 and ε_i, ε_i is the same as in Eq. (1) and uncorrelated with a_1 and ν_i, and Eq. (7) has an adaptive time-varying coefficient C_{i-1}^{T} of dimension $d \times pd^2$. We also have $\hat{a}_0 (= E(a_0))$, the Gaussian $pd^2 \times 1$ initial state vector with covariance matrix $P_{0|0} (= \mathrm{Cov}(a_0))$, and the noise covariance matrices

$$E\{v_k v_i^{\mathrm{T}}\} = Q_k \delta_{k-i}, \tag{8}$$

$$E\{\varepsilon_k \varepsilon_i^{\mathrm{T}}\} = R_k \delta_{k-i}, \tag{9}$$

where T denotes transposition, δ denotes the Kronecker delta sequence, Q_k denotes the covariance matrix of state noise and R_k denotes the covariance matrix of measurement noise. For convenient implementation, $\hat{a}_0$ and $P_{0|0}$ are arbitrarily chosen. Suppose that the evolution law of the state vector a_i is a random walk process which results in a state-space representation below instead of Eqs. (6) and (7):

$$a_{i+1} = a_i + v_i, \tag{10}$$

$$y_i = C_{i-1}^{\mathrm{T}} a_i + \varepsilon_i. \tag{11}$$

Thus, with the aid of a standard Kalman filter the recursive prediction equations

$$P_{i|i-1} = P_{i-1|i-1} + Q_{i-1}, \tag{12}$$

$$\hat{a}_{i|i-1} = \hat{a}_{i-1}, \tag{13}$$

where $P_{i|i-1}$ is the one-step ahead prediction of the state covariance matrix, $P_{i-1|i-1}$ is the estimate (error) covariance matrix of the state vector, $\hat{a}_{i|i-1}$ is the one-step ahead prediction of the state vector, $\hat{a}_{i-1}$ is the optimal filtering estimate of the state vector a_{i-1} and updating equations

$$G_i = P_{i|i-1} C_{i-1} [C_{i-1}^{\mathrm{T}} P_{i|i-1} C_{i-1} + \hat{R}_i]^{-1}, \tag{14}$$

$$P_{i|i} = [I - G_i C_{i-1}^{\mathrm{T}}] P_{i|i-1}, \tag{15}$$

$$\begin{aligned} \hat{a}_{i|i} &:= \hat{a}_i \\ &= \hat{a}_{i|i-1} + G_i (y_i - C_{i-1}^{\mathrm{T}} \hat{a}_{i|i-1}) \end{aligned} \tag{16}$$

can be obtained for $i = 1, 2, \ldots, N$, where G_i is the Kalman gain and the covariance matrix Q_i of state noise is assumed to be known a priori. From the incoming measurement information y_i and the optimal state prediction $\hat{a}_{i|i-1}$ obtained in the previous step, the innovations sequence is defined as

$$z_i := y_i - C_{i-1}^{\mathrm{T}} \hat{a}_{i|i-1}, \tag{17}$$

which leads to the estimate of R_i, using the i most recent residuals, given by

$$\hat{R}_i = \frac{1}{i-1} \sum_{k=1}^{i} (z_k - \bar{z})(z_k - \bar{z})^{\mathrm{T}}, \tag{18}$$

where

$$\bar{z} = \frac{1}{i}\sum_{k=1}^{i} z_k \tag{19}$$

is the mean of the innovations up to the ith time instant. Note that the estimation approach (18) requires the white Gaussian property of z^i. Obviously, this property can be obtained if the Kalman filter operates in its optimum state. Therefore, an adaptive Kalman filter for estimating the state as well as the noise covariance matrices can be called a NAKF.

2.3. Model order selection criteria

Unlike the conventional model order selection procedure based on, say, Akaike information criterion (AIC), the order selection criteria proposed in this section are oriented towards model fitting with load-independent property under varying load conditions. Our extensive tests revealed that model order is the predominant parameter of the NAKF-based time-varying AR model resulting in notable variation of model performance under varying load conditions. In order to select the optimum one, some statistical measures should be applied to evaluate the performance of the MRP under a certain model order.

Let us assume that there are two different load conditions to be encountered during the lifetime of a gearbox, which cover at least N and M inspections respectively, and thus result in two MRP sequences under a certain model order p, MRP(p, i) and MRP(p, j) in correspondence with the two load conditions respectively, where $i = 1, \ldots, N$ and $j = K+1, \ldots, K+M$ and $K \geqslant N$. Here, we assume that the $N+M$ inspections are carried out under the healthy state of the gear of interest.

Then, the ratio between the mean of MRP(p, i) and the mean of MRP(p, j), expressed as

$$R(p) = \frac{\max\left\{\frac{1}{N}\sum_{i=1}^{N}\mathrm{MRP}(p,i), \frac{1}{M}\sum_{j=K+1}^{K+M}\mathrm{MRP}(p,j)\right\}}{\min\left\{\frac{1}{N}\sum_{i=1}^{N}\mathrm{MRP}(p,i), \frac{1}{M}\sum_{j=K+1}^{K+M}\mathrm{MRP}(p,j)\right\}} \tag{20}$$

can be calculated, where it is assumed that we always assign numerator the larger mean of MRP and denominator the smaller one. Thus $R(p)$ is always larger than one given that the numerator and denominator are not equal, we can then obtain the first statistical measure

$$M_1(p) = R(p) - 1 \tag{21}$$

which is positive and should be close to zero when the optimum model order is obtained.

Second, the performance of MRP is expected to be stable and does not present strong variability. Therefore, the root mean square (RMS), as an index of variability, is employed to characterize the dispersion among the MRPs and expressed as

$$s(p) = \sqrt{\frac{1}{N+M-1}\left[\sum_{l=1}^{N+M}\left(\mathrm{MRP}(p,l) - \overline{\mathrm{MRP}}(p)\right)^2\right]}, \tag{22}$$

where $\mathrm{MRP}(p,\ l) = \mathrm{MRP}(p,\ i) \cup \mathrm{MRP}(p,\ j),\ l = 1,\ldots,N+M$, and $\overline{\mathrm{MRP}}(p)$ is the mean of $\mathrm{MRP}(p, l)$ under the order p, given by

$$\overline{\mathrm{MRP}}(p) = \frac{1}{N+M}\sum_{l=1}^{N+M}\mathrm{MRP}(p,l). \tag{23}$$

For consistency with $M_1(p)$ and the following notations, $s(p)$ is replaced by $M_2(p)$, namely

$$M_2(p) = s(p). \tag{24}$$

In principle, $M_2(p)$ should be the smallest under the optimum model order.

Third, the optimum model order should not give rise to significant outliers or abnormally high values of MRP under the healthy state of the gear of interest. Therefore, the kurtosis can be employed to measure the severity of abnormal outliers and gives the statistical measure expressed as

$$M_3(p) = \mathrm{kurtosis}(\mathrm{MRP}(p,l)). \tag{25}$$

The kurtosis function is provided by MATLAB. The value of $M_3(p)$ should be close to or less than three when the optimum model order is obtained. Here, values of $M_3(p)$ less than three are acceptable since only values of kurtosis greater than three indicate the presence of abnormal outliers [16].

Note that the above statistical measures, $M_1(p)$, $M_2(p)$ and $M_3(p)$, are global ones since they take into account both load conditions. For local performance, we still need the same statistical measures to evaluate the performance of the MRP under each load condition so as to obtain acceptable local behavior of the MRP. In such a connection, the following four performance measures are proposed:

$$M_4(p) = \sqrt{\frac{1}{N-1}\left[\sum_{i=1}^{N}\left(\mathrm{MRP}(p,i) - \overline{\mathrm{MRP}}_1(p)\right)^2\right]} \tag{26}$$

and

$$M_5(p) = \sqrt{\frac{1}{M-1}\left[\sum_{j=K+1}^{K+M}\left(\mathrm{MRP}(p,j) - \overline{\mathrm{MRP}}_2(p)\right)^2\right]} \tag{27}$$

are the RMS strengths of $\mathrm{MRP}(p, i)$ and $\mathrm{MRP}(p, j)$ respectively, where $\overline{\mathrm{MRP}}_1(p)$ and $\overline{\mathrm{MRP}}_2(p)$ are the mean values of $\mathrm{MRP}(p, i)$ and $\mathrm{MRP}(p, j)$ under the first and second load conditions and given by $\overline{\mathrm{MRP}}_1(p) = (1/N)\sum_{i=1}^{N}\mathrm{MRP}(p,i)$ and $\overline{\mathrm{MRP}}_2(p) = (1/M)\sum_{j=K+1}^{K+M}\mathrm{MRP}(p,j)$, respectively. Similar to $M_2(p)$, $M_4(p)$ and $M_5(p)$ should be the smallest under the optimum model order.

Furthermore,

$$M_6(p) = \mathrm{kurtosis}(\mathrm{MRP}(p,i)) \tag{28}$$

and

$$M_7(p) = \mathrm{kurtosis}(\mathrm{MRP}(p,j)) \tag{29}$$

are the kurtoses of $\mathrm{MRP}(p, i)$ and $\mathrm{MRP}(p, j)$ respectively. Similar to $M_3(p)$, the values of $M_6(p)$ and $M_7(p)$ should be close to or less than three when the optimum model order is obtained.

It is natural to think and also confirmed by our experiments that the three global statistical measures of MRP, $M_1(p)$, $M_2(p)$ and $M_3(p)$, are the predominant criteria for selecting a model order leading to load-independent model fitting, while the four local statistical measures, $M_4(p)$, $M_5(p)$, $M_6(p)$ and $M_7(p)$, are the auxiliary ones. In case it is difficult to select the proper model order using the global measures, the auxiliary ones should be examined. In the case of fewer inspections available under a certain load condition, the corresponding local statistical measures are less reliable and thus could be ignored. By means of these seven statistical measures together, one can conveniently evaluate the performance of the MRP under a certain model order and thus select the optimum one. In addition, it must be noted that, most of the time, the seven statistical measures cannot simultaneously achieve their target values, therefore a compromised decision must be made.

As well, in view of the multi-component nature of the gear motion residual signals, relatively higher model orders are preferred. Our initial tests indicate that the range of [90,130] is sufficient for selecting the optimum model order which results in load-independence.

3. Experimental validation

3.1. Experimental setup

A mechanical diagnostics test bed (MDTB) as shown in Fig. 2 was utilized in this study to provide data on a commercial transmission as its health progresses from new to faulty and finally to failure. The vibration data used in this study were obtained from the Applied Research Laboratory at the Pennsylvania State University [21]. The MDTB is functionally a motor-drive train-generator test stand [22]. The gearbox is driven at a fixed input speed using a

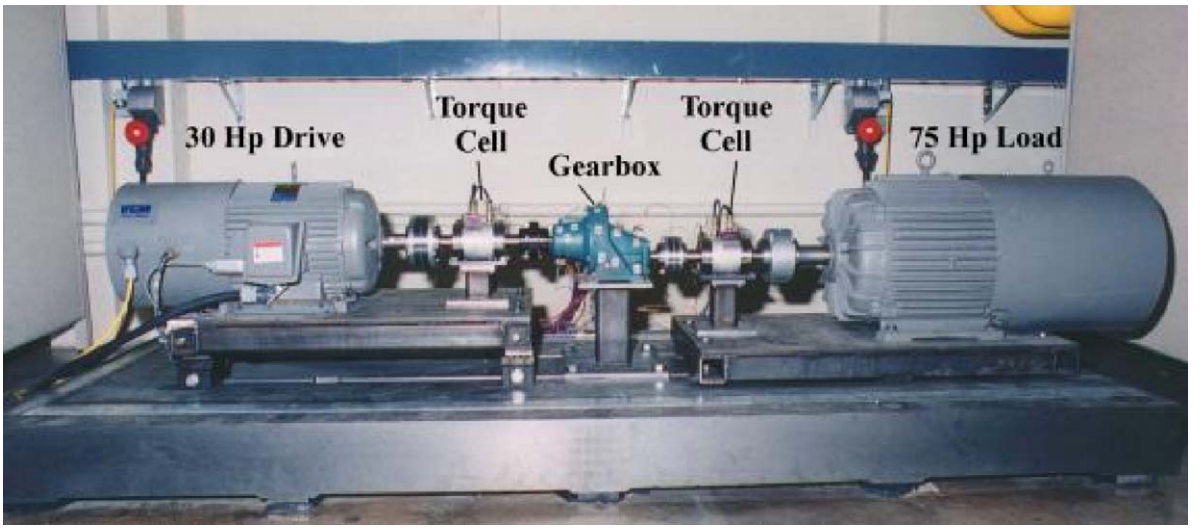

Fig. 2. Mechanical diagnostic test bed (MDTB).

30 hp, 1750 rev/min AC drive motor, and the torque is applied by a 75 hp, 1750 rev/min AC absorption motor. The maximum speed and torque are 3500 rev/min and 225 ft lb respectively. The variation of the torque is accomplished by a vector unit capable of controlling the current output of the absorption motor. The MDTB is highly efficient because the electrical power that is generated by the absorber is fed back to the drive motor. The mechanical and electrical losses are sustained by a small input power. The MDTB has the capability of testing single and double reduction industrial gearboxes with ratios from about 1.2:1 to 6:1. The gearboxes are nominally in the 5–20 hp range. The system is sized to provide the maximum versatility to speed and torque settings. The motors provide about 2–5 times the rated torque of the selected gearboxes, and thus the system can provide good overload capability. Torque-limiting clutches are used on both sides of the gearbox to prevent the transmission of excessive torque as could occur with gear jam or bearing seizure. In addition, torque cells are used on both sides of the gearbox to monitor directly the efficiency and the loads transmitted [22]. The general gearbox information is shown in Table 1.

3.2. Signal processing policy

The tests used in this study include TR#5, TR#8 and TR#10. The tests were conducted with identical single reduction helical 1:1.5 ratio gearboxes which were run at 100% output torque and power for 96 h then increased to 200% or 300% torque and power for a number of hours until failure. In each test, there is a number of unequally spaced inspections performed during the lifetime of each gearbox. Each inspection provides a data file collected in 10-s windows at set times which cover 200,000 sampling points in total and triggered by accelerometer RMS thresholds. The sampling frequency is 20 kHz. Table 2 gives a brief description of the alternating of load conditions for the three tests used in this study.

Fig. 3 shows the locations of accelerometers. The single axis shear piezoelectric accelerometer data A03 for the axial direction is selected in this study to investigate the performance of the proposed model under different failure modes.

Table 1
Gearbox specification of tests TR#5, TR#8 and TR#10

Gearbox ID#	DS3S0150XX
Make	Dodge APG
Model	R86001
Rated input speed	1750 rev/min
Maximum rated output torque	528 in lb
Maximum rated input hp	10.0
Gear ratio	1.533
Contact ratio	2.388
Gear mesh frequency of driven gear (Hz)	875.53
Gear mesh frequency of pinion gear (Hz)	874.99
Number of teeth (driven gear)	46
Number of teeth (pinion gear)	30

Table 2
Load conditions[a]

Condition	Input speed (rev/min)	Output torque (in lb)	Power (hp)	Duration (h)
#1	1750	540	9.8	96.0
#2	1750	1620/1080/1080	20/30/20	51.5/6/81.1

[a]Note: Output torque (in lb) 1620/1080/1080 denotes the loads for tests TR#5, TR#8 and TR#10, respectively. Same for power (hp) and duration (h).

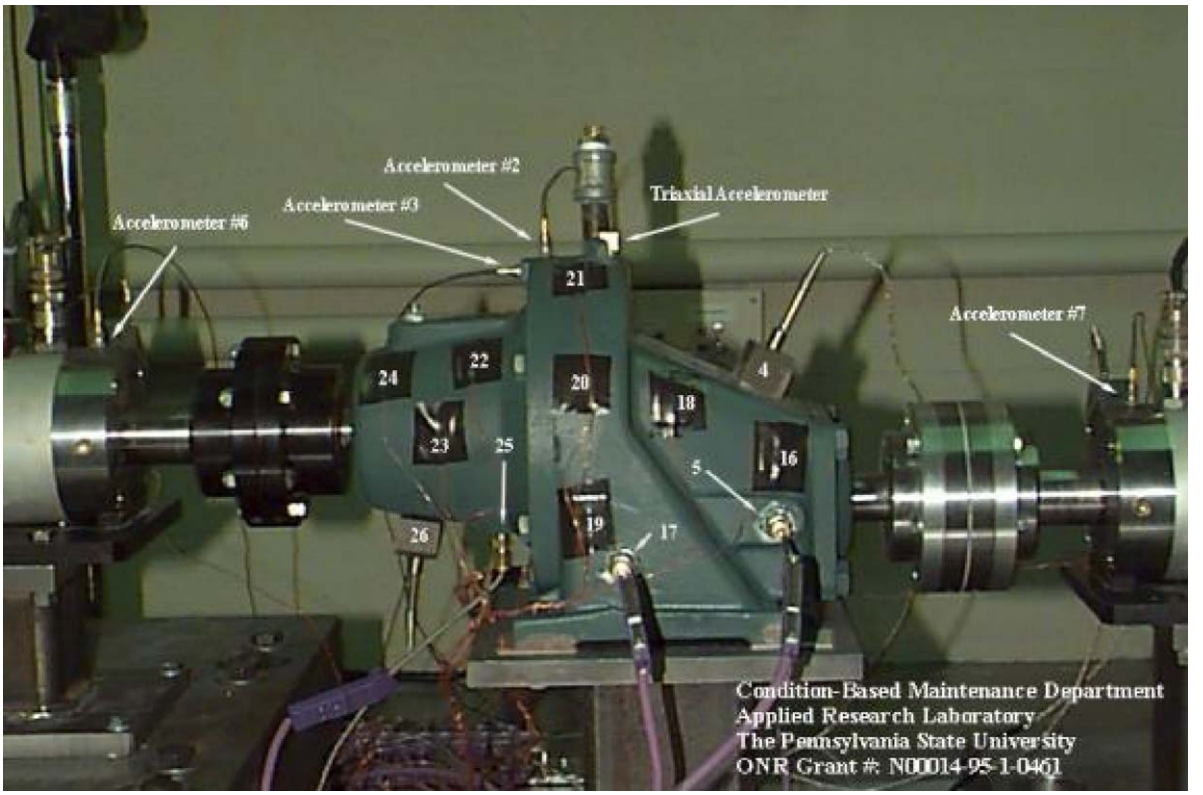

Fig. 3. Distribution of accelerometers.

The proposed MRP will be compared with the fault-growth parameter (FGP) proposed by Miller [23], AR model residual kurtosis and gear motion residual kurtosis. For convenience, the abbreviations RMS1, RMS2, RMS3, MRK1 and MRK2 will be used to denote the RMS strengths of AR model residuals, gear motion residual signals, TSA signals, AR model residual kurtosis and gear motion residual kurtosis, respectively. Also, the three standard deviations of the baseline AR model residuals, determined at the beginning of each test by using the gear motion residual signal of the first inspection, is a constant throughout each test.

4. Model evaluation

Three types of faults, two adjacent gear tooth failures, two non-adjacent gear tooth failures, and distributed gear tooth failures, are investigated in this study. Unlike in the previous studies, e.g. [7,10,11], the gear faults in this study were not intentionally created in advance. The gearbox in each test was driven under varying load conditions until some abnormal values of the RMS and kurtosis of the raw vibration signals were present. The MDTB was then shut down and the gearbox was open by technicians to check the root cause which triggered the abnormal values of these monitoring indexes. The gear of interest is always the driven gear since its failure was found to be the only factor which caused the MDTB to shut down. In the present study, we investigate the TR#5, TR#8 and TR#10 corresponding to the three types of faults mentioned above, respectively. We note that the same classification of gear faults was used to investigate the MDTB test runs in Refs. [16,23].

4.1. Two adjacent gear tooth failures (TR#5)

The gearbox in this test was driven until there was a break in two adjacent teeth of the driven gear (see Fig. 4 for a photograph of the broken gear). There was a total of 83 data files collected

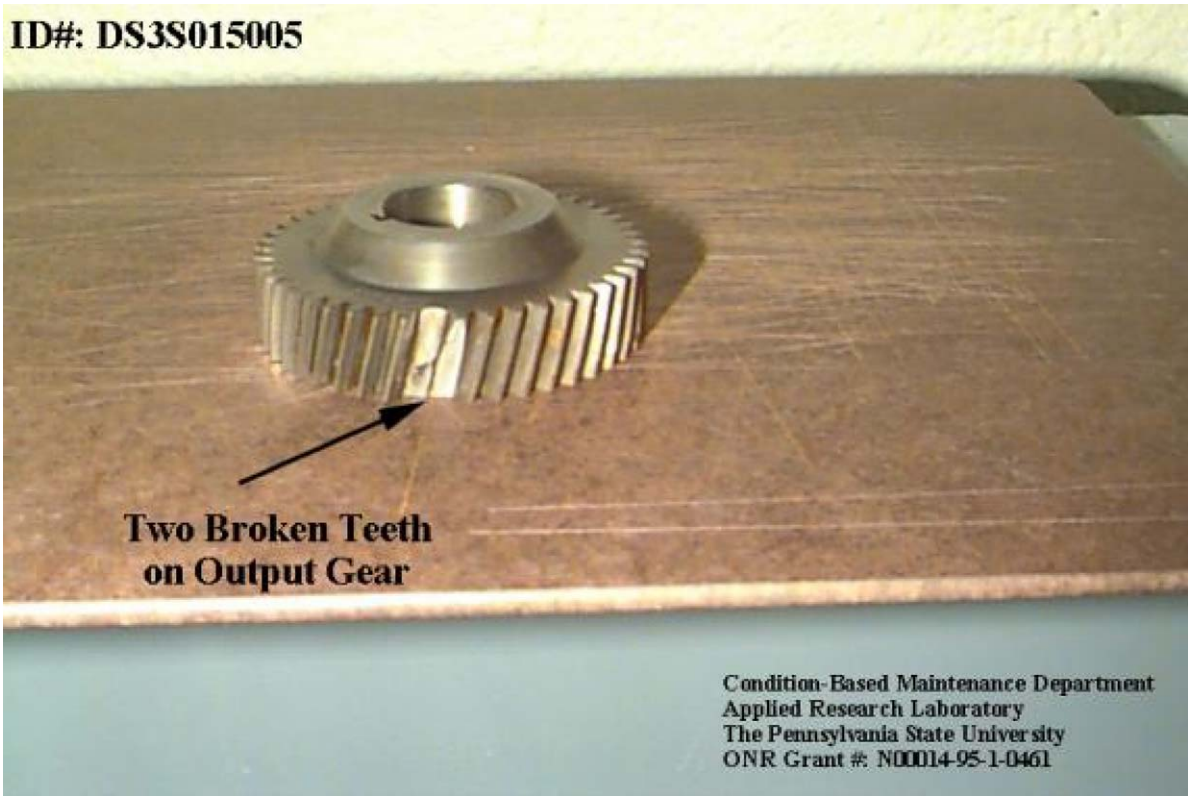

Fig. 4. Two adjacent gear tooth failures of the driven gear in test TR#5.

during the lifetime of this test. The output torque level was 540 in lb before file 13 and switched to 1620 in-lb from file 13 as shown in Fig. 6(a).

For this test, 12 gear motion residual signals under the first load condition of 540 in lb and the first 40 gear motion residual signals under the second load condition of 1620 in lb are used to determine the optimum AR model order. The initial inspection of $M_1(p)$, $M_2(p)$ and $M_3(p)$ as shown in Figs. 5(a), (b) and (c) respectively, indicates that the optimum AR model order could be selected from 100, 110 and 117. In detail, Fig. 5(a) shows that the order of 110 gives the smallest value of $M_1(p)$. Fig. 5(b) shows that the order of 100 is the best when using $M_2(p)$, and in Fig. 5(c), both $M_3(100)$ and $M_3(110)$ are less than 3, but $M_3(117)$ gives a value of kurtosis, 3.818 which is the largest among the kurtosis values of these three orders. Thus, the order of 117 is excluded. Further examination of $M_6(p)$ and $M_7(p)$ in Figs. 5(f) and (g) shows no notable difference between order 100 and 110, whereas $M_4(100)$ and $M_5(100)$ in Figs. 5(d) and (e) have smaller RMS values in comparison with $M_4(110)$ and $M_5(110)$. Therefore, an AR(100) model is selected for this test.

In Figs. 6 and 7, the two vertical dashed lines in each subplot denote the switch of load condition from data file 12 to 13. As shown in Figs. 6(b) and (c), both RMS1 and RMS2 indicate that the time instant corresponding to the presence of incipient fault is around file 74. Unfortunately, RMS3 as shown in Fig. 6(d) not only fails to reveal the occurrence time of the incipient fault but shows a significant load-dependent variation around file 12. Moreover, load-dependence is also observed in RMS2, as clearly shown around file 12 in Fig. 6(c). Therefore, RMS1 shows the best performance when compared with RMS2 and RMS3.

Fig. 7 shows the comparison between the proposed MRP and other state parameters. As shown in Fig. 7(a), the MRP level is very low between file 1 and 71, it is independent of varying load conditions as indicated by the arrow mark, and there is no varying-load-induced jump at the switch point of load condition indicated by the two vertical dashed lines. After the incipient fault initiates around file 73, the MRP jumps to a higher level. We remark here that a justifiable evaluation of the performance of FGP should not take into account condition #1 (540 in lb output torque level) since the FGP could be highly load-dependent as shown in Fig. 7(b). Therefore, correct diagnosis by the FGP should assess the state of the driven gear by checking the deviation from the baseline pattern when the driven gear is in its healthy state under load condition #2.

Further, in view of the load-independence of the MRP, we evaluate its performance under the healthy state of the driven gear by considering all data files before the occurrence of the incipient fault. Thus, further investigation denotes that mean values of the MRP within file ranges [72,82] and [1,71] are 1.799% and 0.1608%, respectively, which result in a ratio of 11.19. On the other hand, the FGP shown in Fig. 7(b) demonstrates very serious load-dependent behavior and a dramatic jump is clearly present as indicated by the arrow mark at the load switch point from file 12 to 13. Even though the FGP goes up quickly to a level higher than the MRP during the intermediate and advanced faulty states within file range [72,82], 10.26% and 1.079%, i.e. mean values of FGP within file ranges [72,82] and [13,71] respectively, resulting in a ratio of 9.510 which is obviously less than the 11.19 of the MRP. Thus, this phenomenon implies that the fault-induced feature embedded in the AR model residuals is further amplified in comparison with the decomposed gear motion signal proposed by Wang and McFadden [1]. Additionally, considerable variability is present in the traces of MRK1 and MRK2 as shown in Figs. 7(c) and (d), respectively. Moreover, kurtosis values associated with the healthy state of the driven gear are equal to or higher than the kurtosis values associated with the intermediate faulty state of the

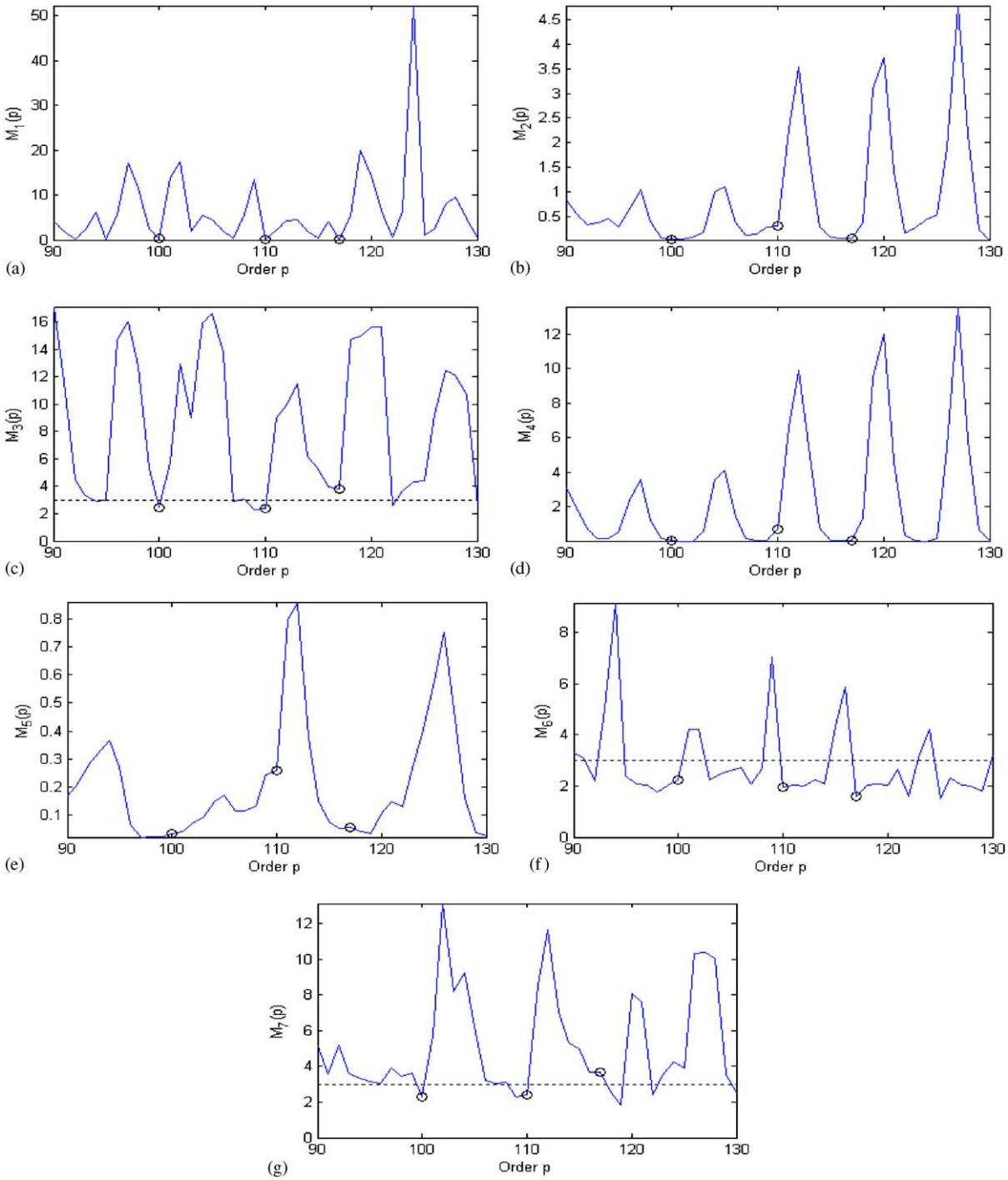
(a)
M1(p)
Order p
(b)
M2(p)
Order p
(c)
M3(p)
Order p
(d)
M4(p)
Order p
(e)
M5(p)
Order p
(f)
M6(p)
Order p
(g)
M7(p)
Order p

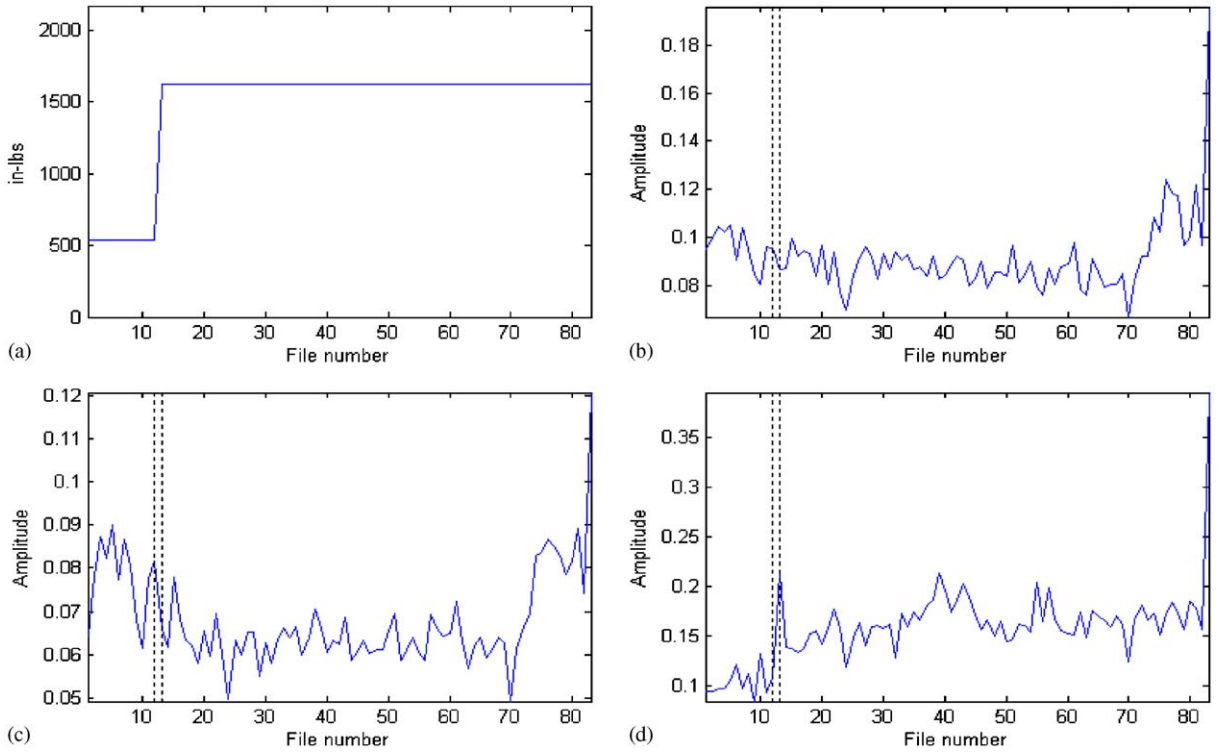

Fig. 6. Load condition, RMS1, RMS2 and RMS3 vs. data file of test TR#5. The two vertical dashed lines in subplots (b), (c), and (d) denote the switch of load condition from data file 12 to 13. (a) Load condition (output torque); (b) RMS of AR model residual signal (RMS1); (c) RMS of gear motion residual signal (RMS2); (d) RMS of TSA signal (RMS3).

driven gear due to its strong sensitivity to outliers. This is inconsistent with the actual state evolution of the driven gear. Further comparison reveals that MRK1 shows less variability than MRK2 within file range [1,71]. The reason is that AR model residuals are much less load-dependent in comparison with gear motion residual signals. Therefore, the proposed MRP possesses remarkable advantages over the other three state parameters in this case.

4.2. Two non-adjacent gear tooth failures (TR#8)

The gearbox in this test was driven until there was a break in two non-adjacent teeth of the driven gear (see Fig. 8 for a photograph of the broken gear). There is a total of 145 data files

Fig. 5. Statistical measures of MRP for model order selection of test TR#5: (a) Ratio-based $M_1(p)$ for two load conditions, $M_1(100) = 0.2600$, $M_1(110) = 0.1484$, $M_1(117) = 0.1654$; (b) ratio-based $M_2(p)$ for two load conditions, $M_2(100) = 0.0304$, $M_2(110) = 0.3087$, $M_2(117) = 0.0516$; (c) Kurtosis-based $M_3(p)$ for two load conditions, $M_3(100) = 2.4505$, $M_3(110) = 2.3905$, $M_3(117) = 3.8183$; (d) RMS-based $M_4(p)$ for load condition #1, $M_4(100) = 0.0137$, $M_4(110) = 0.7059$, $M_4(117) = 0.0277$; (e) RMS-based $M_5(p)$ for load condition #2, $M_5(100) = 0.0333$, $M_5(110) = 0.2578$, $M_5(117) = 0.0562$; (f) Kurtosis-based $M_6(p)$ for load condition #1, $M_6(100) = 2.2560$, $M_6(110) = 1.9611$, $M_6(117) = 1.5913$; (g) Kurtosis-based $M_7(p)$ for load condition #2, $M_7(100) = 2.2948$, $M_7(110) = 2.3852$, $M_7(117) = 3.6814$.

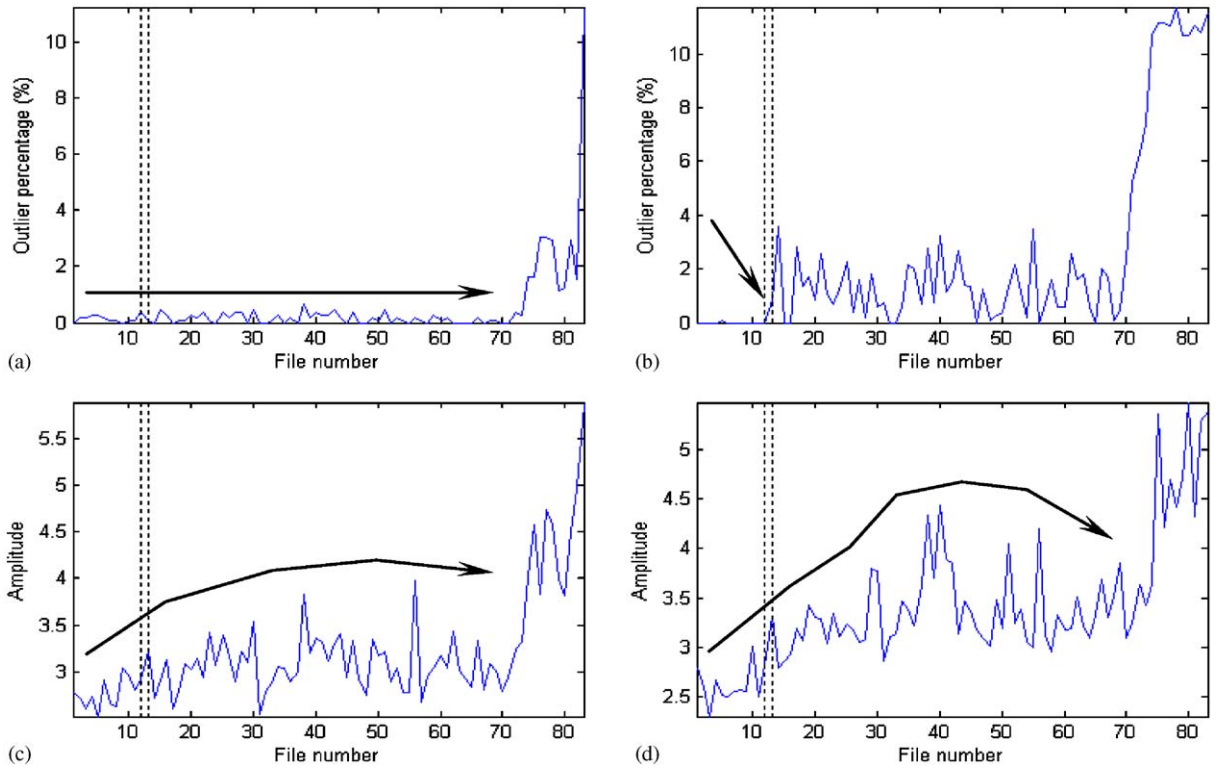

Fig. 7. MRP, FGP, MRK1 and MRK2 vs. data file of test TR#5. The two vertical dashed lines in each subplot denote the switch of load condition from data file 12 to 13. (a) AR model residuals-based machine state deterioration parameter (MRP), where the arrow line denotes the general trend of MRP; (b) fault growth parameter (FGP), where the arrow mark denotes the load switch-induced jump of FGP; (c) AR model residual kurtosis (MRK1), where the arrow curve denotes the general trend of MRK1; (d) gear motion residual kurtosis (MRK2), where the arrow curve denotes the general trend of MRK2.

collected during the lifetime of this test. The output torque level was 540 in lb before file 39 and switched to 1080 in lb from file 39 as shown in Fig. 10(a).

For this test, the first 35 gear motion residual signals under the first load condition of 540 in lb and the first 10 gear motion residual signals under the second load condition of 1080 in lb are used to determine the optimum AR model order. The initial inspection of $M_1(p)$, $M_2(p)$ and $M_3(p)$ as shown in Figs. 9(a), (b) and (c) respectively, indicates that the optimum AR model order could be selected from 104, 105, 106, 107 and 120. In Fig. 9(a), order 120 gives the smallest $M_1(p)$ value of 0.0130 and shows a remarkable advantage over the other four orders. In Fig. 9(b), $M_2(120)$ is slightly larger than the smallest $M_2(106)$. In addition, in Fig. 9(e), $M_5(120)$ is not the smallest but shows a value of 0.0724 which is very consistent with the value of $M_4(120)$ equal to 0.0743. Such a fact implies that order 120 results in the same variability under the two load conditions. The kurtosis-based measures $M_3(p)$, $M_6(p)$ and $M_7(p)$ as shown in Figs. 9(c), (f) and (g) do not show notable difference among these five order values except that $M_7(105)$ gives a relatively higher kurtosis value of 4.558. Therefore, an AR(120) model is selected for this test.

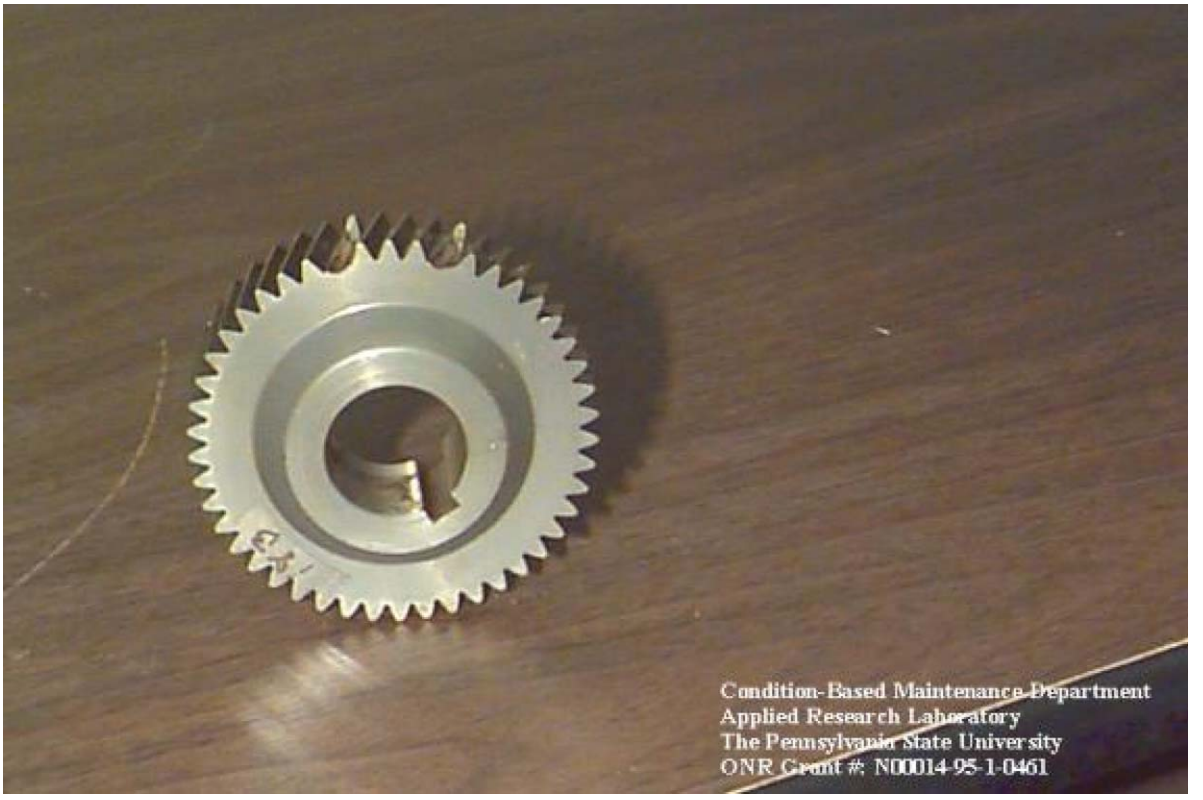

Fig. 8. Two non-adjacent gear tooth failures of the driven gear in test TR#8.

In Figs. 10 and 11, the two vertical dashed lines in each subplot denote the switch of load condition from data file 38 to 39. As shown in Figs. 10(b) and (c), RMS1 and RMS2 demonstrate two very consistent descriptions of the state progression of the driven gear, from which the occurrence time of the incipient fault can clearly be seen around file 54. However, RMS3 shows a generally (but not monotonically) ascending trend with the increase of time, where the occurrence time of incipient fault is rather ambiguous.

The proposed MRP shown in Fig. 11(a) agrees well with the FGP in Fig. 11(b) with respect to the indication of the occurrence time of the incipient fault around file 54 which is also consistent with the findings from RMS1 and RMS2 as shown in Figs. 10(b) and (c), respectively. However, the MRP develops at a relatively constant level before file 54 when the driven gear is in its healthy state and shows no load-dependent behavior at the load switch point denoted by the two vertical dashed lines in Fig. 11(a), whereas there is an apparent indication of load-dependent variation in the trace of the FGP at file 39 to 40 when the load is switched to 1080 in lb as indicated by the arrow mark at the load switch point denoted by the two vertical dashed lines in Fig. 11(b). In addition, comparing the scale values of ordinates in Fig. 11(a) of the MRP and Fig. 11(b) of the FGP respectively, it can be found that the values of the MRP are much larger than those of the FGP under the faulty state of gearbox within file range [54,145]. Further investigation reveals that

means of the MRP within file ranges [54,145] and [1,53] are 11.47% and 0.2657%, respectively, which result in a ratio of 33.12. On the other hand, the ratio obtained from file ranges [54,145] and [39,53] of the FGP is 18.57 which is significantly less than 33.12. Therefore, the gear

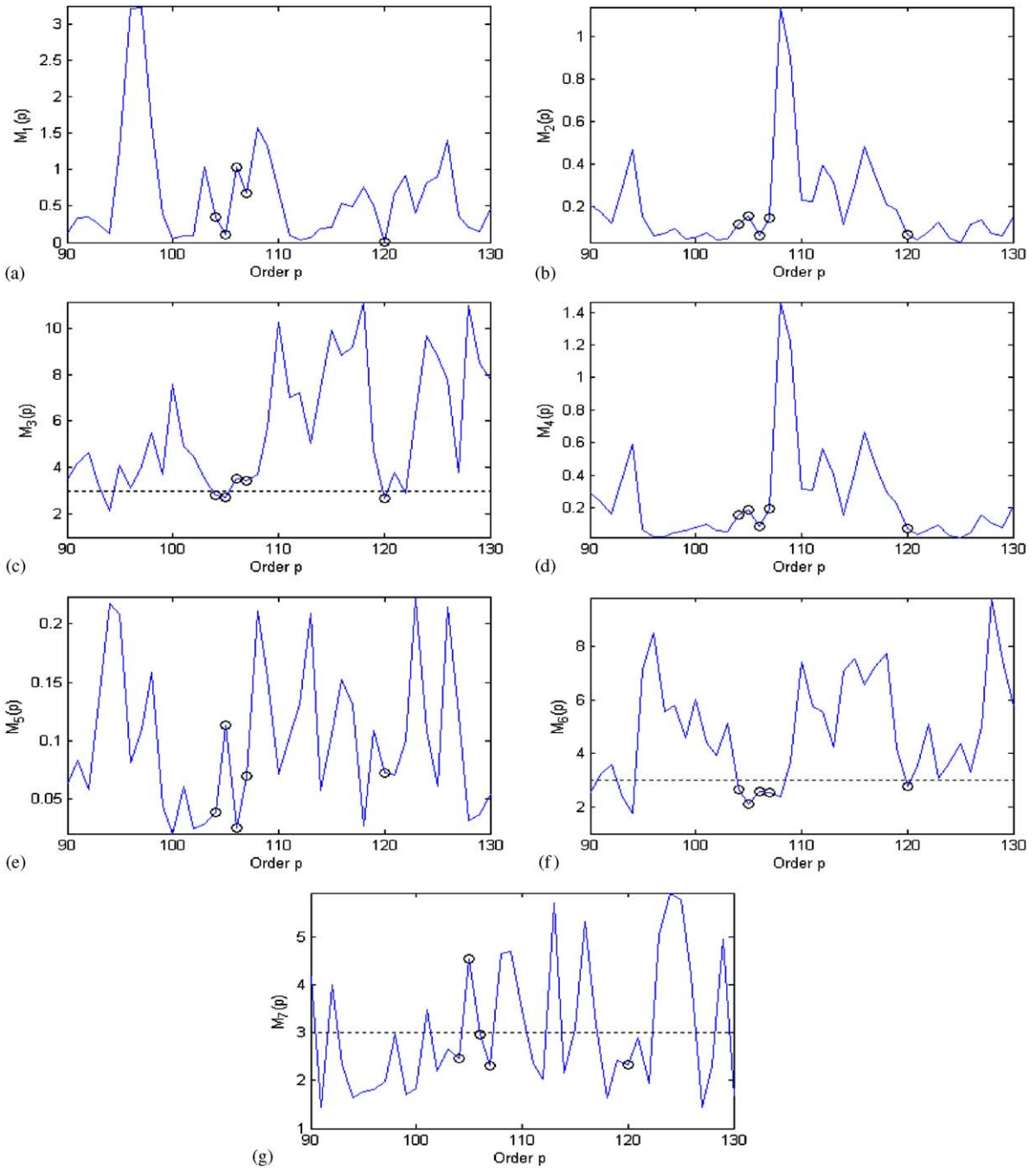

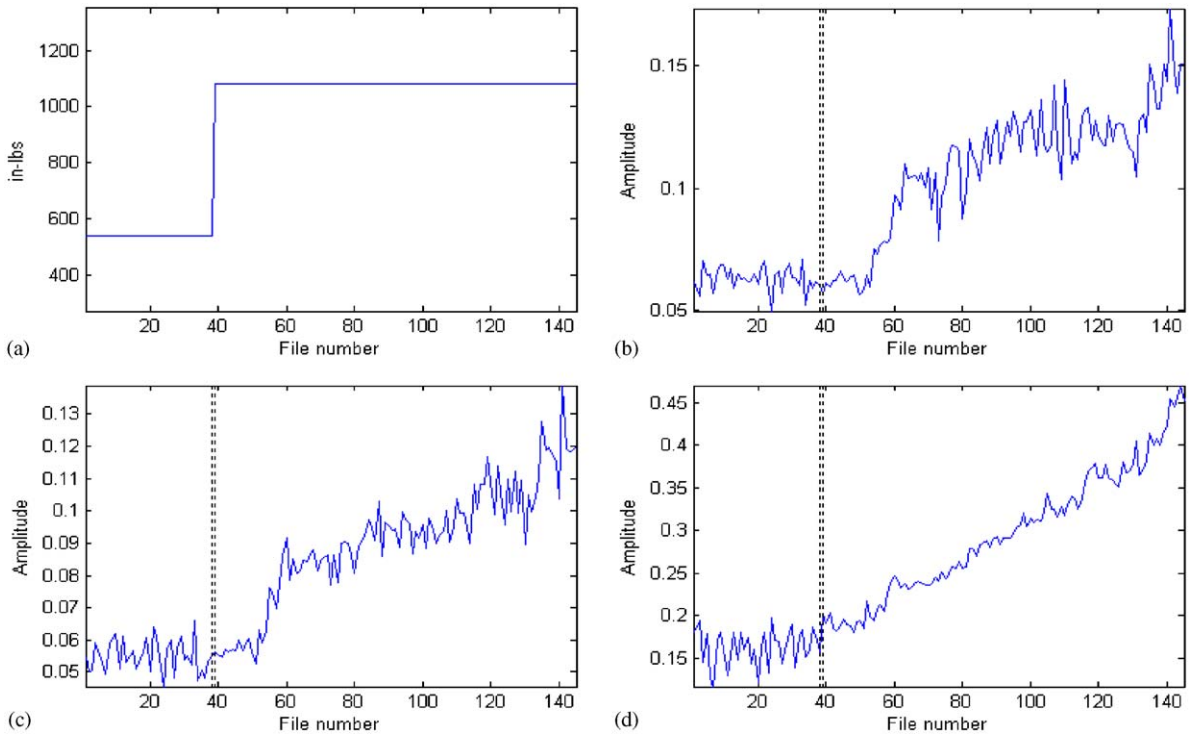

Fig. 10. Load condition, RMS1, RMS2 and RMS3 vs. data file of test TR#8. The two vertical dashed lines in subplots (b), (c), and (d) denote the switch of load condition from data file 38 to 39. (a) Load condition (output torque); (b) RMS of AR model residual signal (RMS1); (c) RMS of gear motion residual signal (RMS2); (d) RMS of TSA signal (RMS3).

fault-induced feature is strongly enhanced by the MRP in comparison with the FGP. As shown in Figs. 11(c) and (d), MRK1 and MRK2 yield indication of the incipient fault around file 59 as indicated by the arrow marks which is somewhat later than those of the MRP and FGP. As well, considerable variability is present in the traces of MRK1 and MRK2. Therefore, the MRP presents the best description of the state development of the driven gear in this test.

Fig. 9. Statistical measures of MRP for model order selection of test TR#8. (a) Ratio-based $M_1(p)$ for two load conditions, $M_1(104) = 0.3503$, $M_1(105) = 0.1082$, $M_1(106) = 1.0388$, $M_1(107) = 0.6714$, $M_1(120) = 0.0130$; (b) ratio-based $M_2(p)$ for two load conditions, $M_2(104) = 0.1178$, $M_2(105) = 0.1581$, $M_2(106) = 0.0658$, $M_2(107) = 0.1498$, $M_2(120) = 0.0696$; (c) Kurtosis-based $M_3(p)$ for two load conditions, $M_3(104) = 2.8130$, $M_3(105) = 2.7091$, $M_3(106) = 3.5365$, $M_3(107) = 3.4545$, $M_3(120) = 2.6903$; (d) RMS-based $M_4(p)$ for load condition #1, $M_4(104) = 0.1570$, $M_4(105) = 0.1909$, $M_4(106) = 0.0844$, $M_4(107) = 0.1924$, $M_4(120) = 0.0743$; (e) RMS-based $M_5(p)$ for load condition #2, $M_5(104) = 0.0387$, $M_5(105) = 0.1132$, $M_5(106) = 0.0252$, $M_5(107) = 0.0702$, $M_5(120) = 0.0724$; (f) Kurtosis-based $M_6(p)$ for load condition #1, $M_6(104) = 2.6595$, $M_6(105) = 2.1253$, $M_6(106) = 2.5559$, $M_6(107) = 2.5509$, $M_6(120) = 2.7659$; (g) Kurtosis-based $M_7(p)$ for load condition #2, $M_7(104) = 2.4681$, $M_7(105) = 4.5576$, $M_7(106) = 2.9697$, $M_7(107) = 2.3241$, $M_7(120) = 2.3291$.

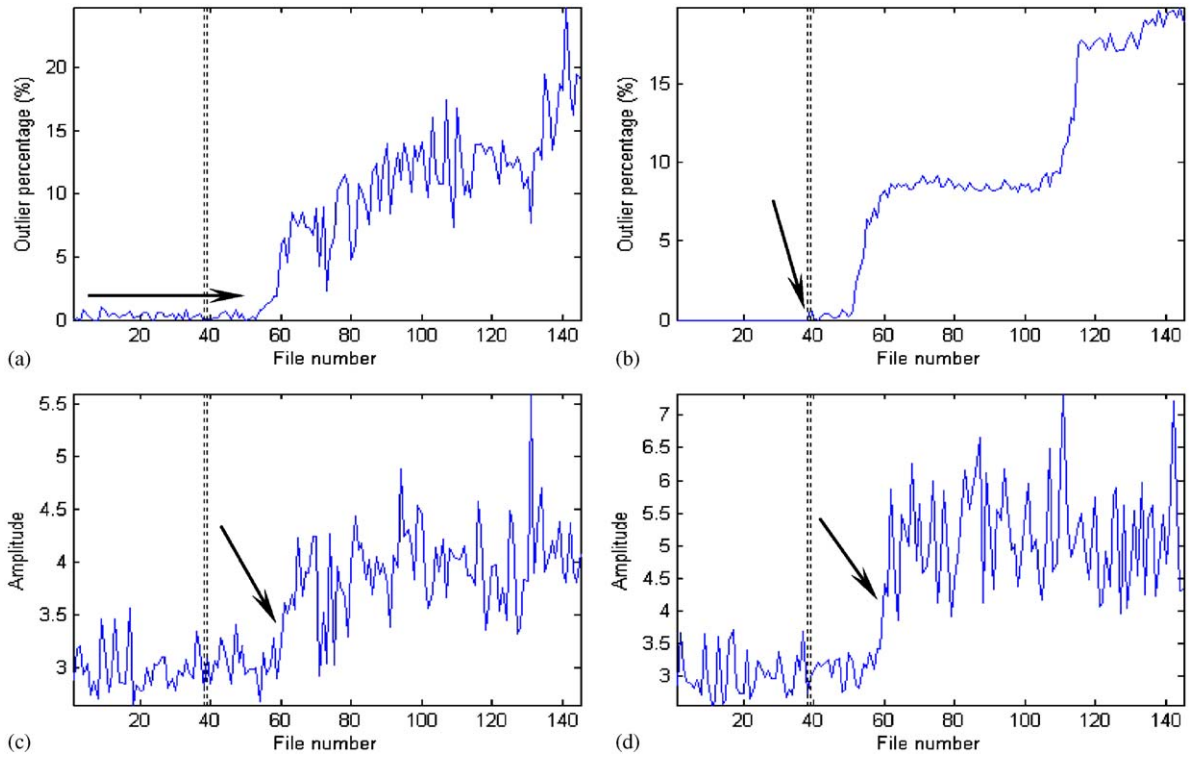

Fig. 11. MRP, FGP, MRK1 and MRK2 vs. data file of test TR#8. The two vertical dashed lines in each subplot denote the switch of load condition from data file 38 to 39. (a) AR model residuals-based machine state deterioration parameter (MRP), where the arrow line denotes the general trend of MRP; (b) fault growth parameter (FGP), where the arrow mark denotes the load switch-induced jump of FGP; (c) AR model residual kurtosis (MRK1), where the arrow mark denotes the first indication of incipient fault around data file 59; (d) gear motion residual kurtosis (MRK2), where the arrow mark denotes the first indication of incipient fault around data file 59.

4.3. Distributed gear tooth failures (TR#10)

The gearbox in this test was driven until there was a break in distributed teeth of the driven gear (see Fig. 12 for a photograph of the broken gear). There is a total of 148 data files collected during the lifetime of this test. The output torque level was 540 in lb before file 13 and switched to 1080 in lb from file 13 as shown in Fig. 14(a).

For this test, the first 10 gear motion residual signals under the first load condition of 540 in lb and the first 10 gear motion residual signals under the second load condition of 1080 in lb are used to determine the optimum AR model order. The initial inspection of $M_1(p)$, $M_2(p)$ and $M_3(p)$ as shown in Figs. 13(a), (b) and (c) respectively, indicates that the optimum AR model order could be selected from 97, 98, 99, 106 and 107. On examining Fig. 13(a), one can find that $M_1(97)$ and $M_1(98)$ are the smallest two values, $M_1(99)$ and $M_1(106)$ are very close to each other, whereas $M_1(107)$ gives the largest value. However, further inspection of the RMS-based $M_2(p)$ and $M_4(p)$ as shown in Figs. 13(b) and (d) indicates that order 107 gives the smallest $M_2(p)$ and $M_4(p)$ among

Fig. 12. Distributed gear tooth failures of the driven gear in test TR#10.

the five orders. The RMS-based $M_5(p)$ as shown in Fig. 13(e) shows a very slight difference between $M_5(106)$ and $M_5(107)$. As well, on examining the kurtosis-based $M_3(p)$, $M_6(p)$ and $M_7(p)$ in Figs. 13(c), (f) and (g), no remarkable difference is present among the orders of 97, 98, 99 and 107. They all give kurtosis values close to 3, but the order of 106 results in a relatively higher kurtosis, 4.890, in $M_3(p)$ as shown in Fig. 13(c). Therefore, considering the smallest variability of the order of 107, an AR(107) model is selected for this test.

In Figs. 14 and 15, the two vertical dashed lines in each subplot denote the switch of load condition from data file 12 to 13. As seen in Figs. 14(b) and (c), RMS1 and RMS2 yield very similar descriptions of the state development of the driven gear. The occurrence time of the incipient fault can be identified at file 38. However, RMS3 shown in Fig. 14(d) highlights the existence of the fault much later than RMS1 and RMS2. The alarm can only be obtained at file 140.

In this case, the proposed MRP as shown in Fig. 15(a) demonstrates remarkable advantages over the FGP, MRK1 and MRK2. The trace of the MRP within file range [1, 37] shows no load-dependent behavior under the healthy stage of gearbox as indicated by the arrow mark in Fig. 15(a) and progress at a considerably higher level after file 38 when the incipient fault initiates. As indicated by the scale values of the ordinate in Fig. 15(a), the MRP gives very high values

which are usually larger than 10% and may be as high as 70% under the faulty state of the gearbox within file range [38, 148]. However, as shown in Fig. 15(b), the FGP shows its values mainly between 5% and 25%. Therefore, the gear fault-induced feature is again significantly

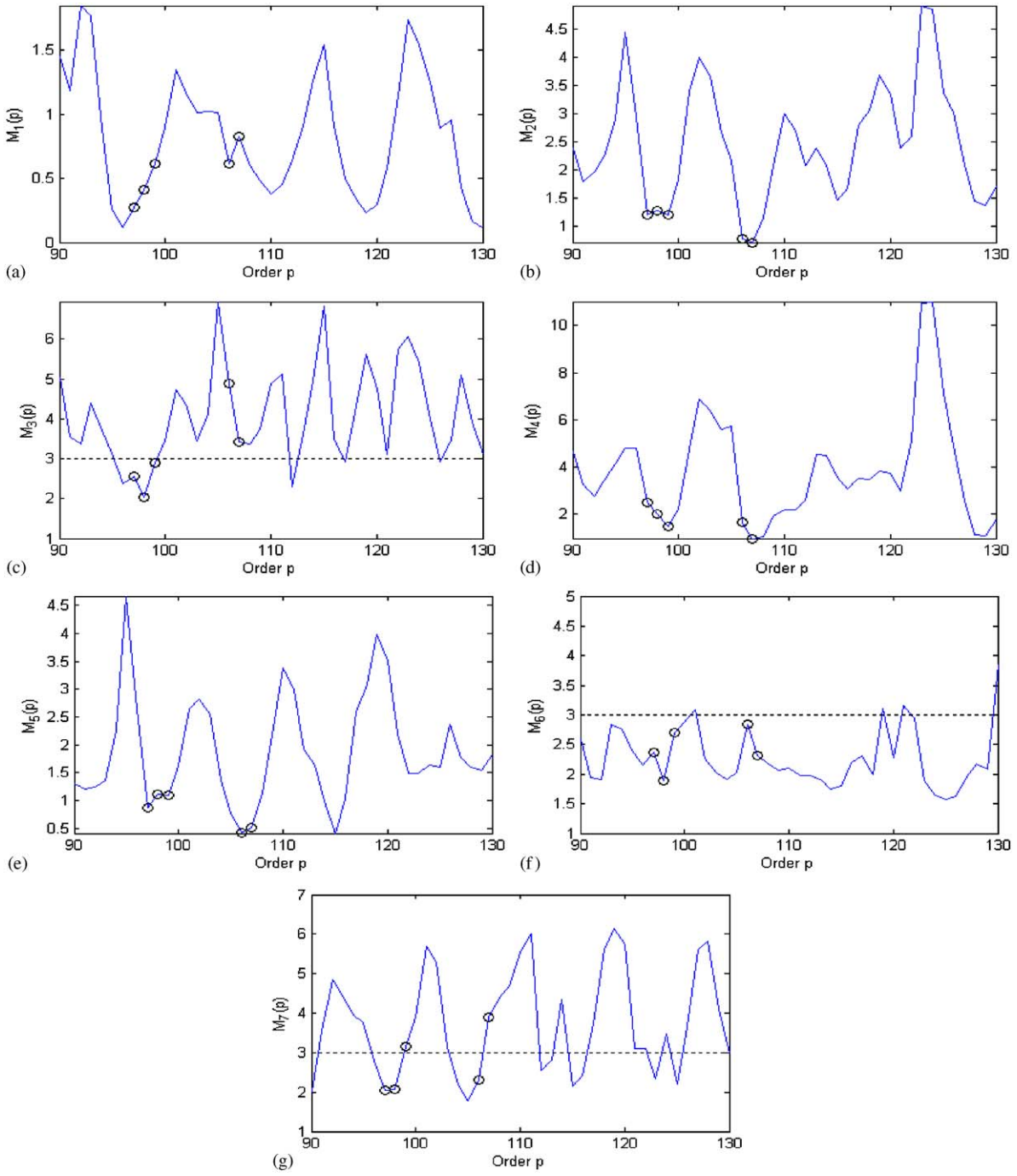

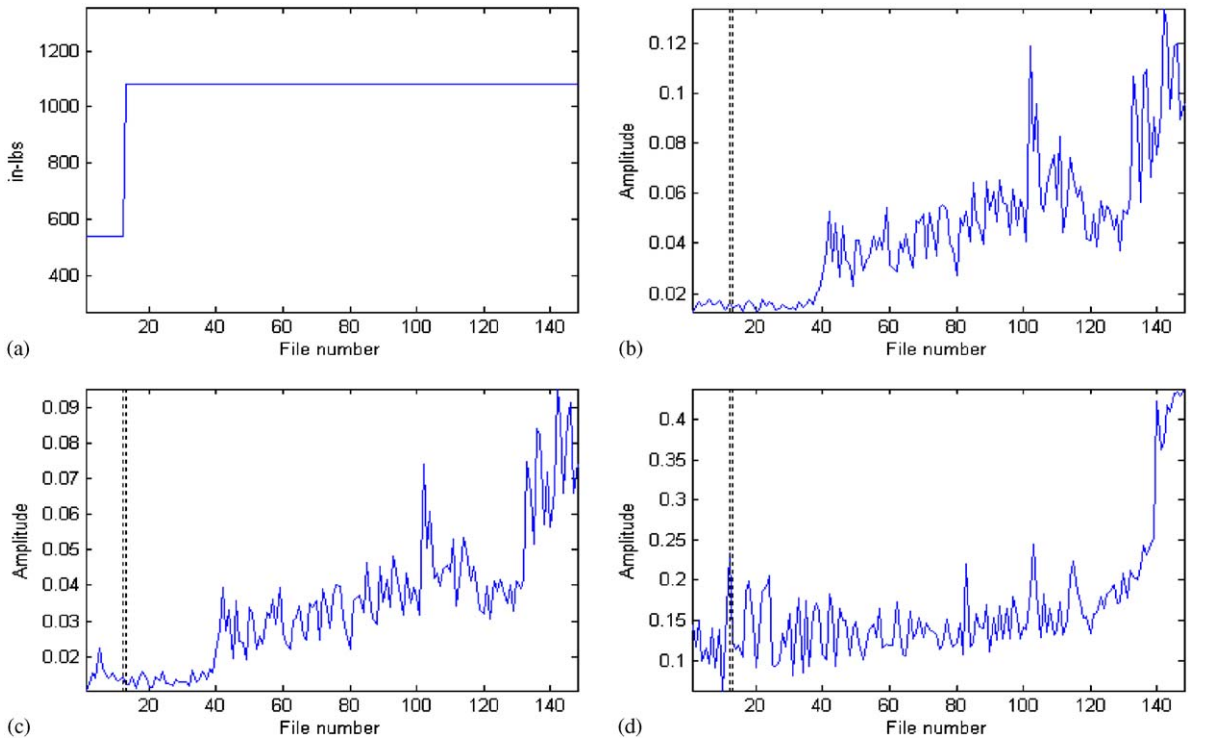

Fig. 14. Load condition, RMS1, RMS2 and RMS3 vs. data file of test TR#10. The two vertical dashed lines in subplots (b), (c), and (d) denote the switch of load condition from data file 12 to 13: (a) Load condition (output torque); (b) RMS of AR model residual signal (RMS1); (c) RMS of gear motion residual signal (RMS2); (d) RMS of TSA signal (RMS3).

enhanced in MRP. Following the same analysis as in the previous cases, the MRP in this case yields a ratio of 28.01 which is larger than the ratio of 24.30 of the FGP. Thus, the fault-induced feature is also improved in the AR model residuals as well as an efficient elimination of load-dependent behavior which, however, is slightly present in the trace of the FGP after the load condition is switched to 1080 in lb as shown by the arrow mark in Fig. 15(b). In addition, MRK1 and MRK2 show dramatic decreases when the fault develops to its intermediate stage, for

Fig. 13. Statistical measures of MRP for model order selection of test TR#10: (a) ratio-based $M_1(p)$ for two load conditions, $M_1(97) = 0.2751$, $M_1(98) = 0.4105$, $M_1(99) = 0.6160$, $M_1(106) = 0.6118$, $M_1(107) = 0.8310$; (b) ratio-based $M_2(p)$ for two load conditions, $M_2(97) = 1.1903$, $M_2(98) = 1.2771$, $M_2(99) = 1.1977$, $M_2(106) = 0.7758$, $M_2(107) = 0.7051$; (c) Kurtosis-based $M_3(p)$ for two load conditions, $M_3(97) = 2.5509$, $M_3(98) = 2.0347$, $M_3(99) = 2.8979$, $M_3(106) = 4.8896$, $M_3(107) = 3.4301$; (d) RMS-based $M_4(p)$ for load condition #1, $M_4(97) = 2.5027$, $M_4(98) = 2.0062$, $M_4(99) = 1.4783$, $M_4(106) = 1.6361$, $M_4(107) = 0.9682$; (e) RMS-based $M_5(p)$ for load condition #2, $M_5(97) = 0.8762$, $M_5(98) = 1.1181$, $M_5(99) = 1.0971$, $M_5(106) = 0.4151$, $M_5(107) = 0.5130$; (f) Kurtosis-based $M_6(p)$ for load condition #1, $M_6(97) = 2.3735$, $M_6(98) = 1.8913$, $M_6(99) = 2.6992$, $M_6(106) = 2.8436$, $M_6(107) = 2.3067$; (g) Kurtosis-based $M_7(p)$ for load condition #2, $M_7(97) = 2.0364$, $M_7(98) = 2.0634$, $M_7(99) = 3.1509$, $M_7(106) = 2.3034$, $M_7(107) = 3.8856$.

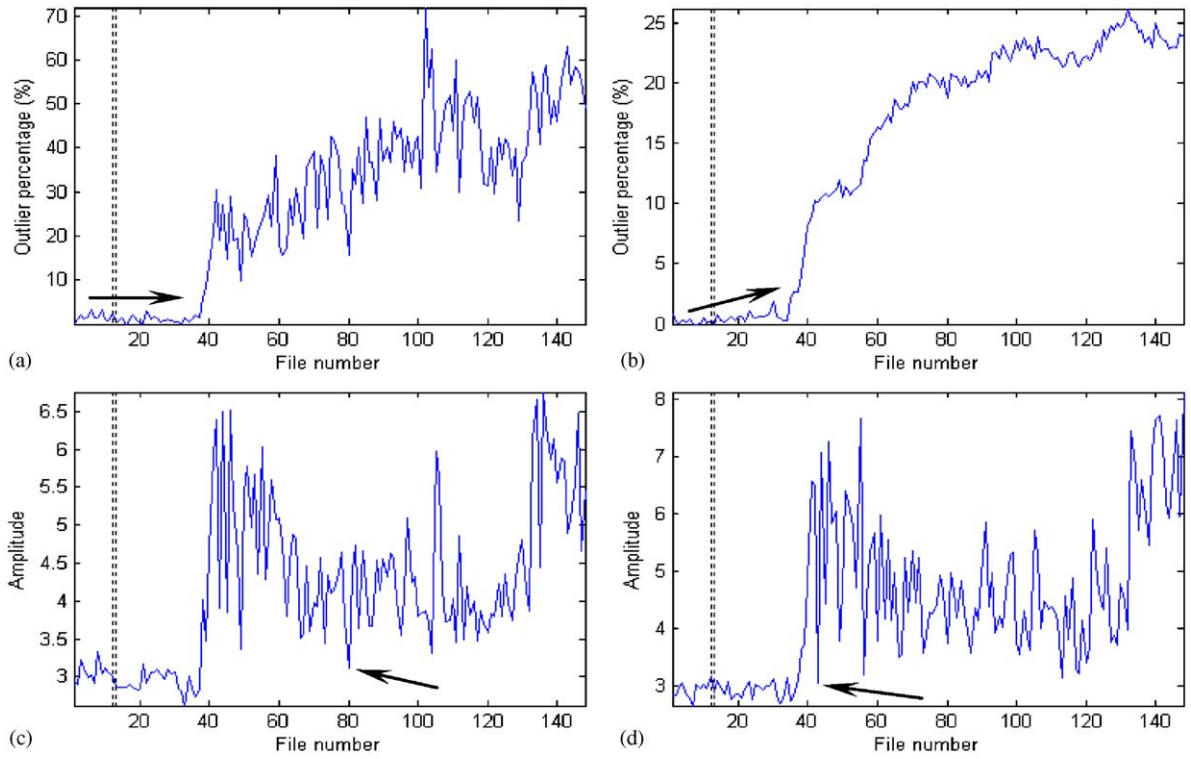

Fig. 15. MRP, FGP, MRK1 and MRK2 vs. data file of test TR#10. The two vertical dashed lines in each subplot denote the switch of load condition from data file 12 to 13: (a) AR model residuals-based machine state deterioration parameter (MRP), where the arrow line denotes the general trend of MRP; (b) fault growth parameter (FGP), where the arrow line denotes the general trend of FGP; (c) AR model residual kurtosis (MRK1), where the arrow mark denotes the dramatic decrease of MRK1 at the intermediate fault stage; (d) gear motion residual kurtosis (MRK2), where the arrow mark denotes the dramatic decrease of MRK2 at the intermediate fault stage.

example, as indicated by the arrow marks in Figs. 15(c) and (d), and thus yield erroneous indications of the stage of the driven gear, although the occurrence time of the incipient fault can be identified around file 38 as shown in Figs. 15(c) and (d) respectively.

5. Conclusions

In this study, a highly efficient and robust state parameter extracted using adaptive AR modeling is proposed for detecting state development of gearboxes under varying load conditions. This technique is independent of load and able to yield a more reliable and stable measure of the state of the gear of interest under varying load conditions, compared with other techniques recently proposed in related studies.

In particular, it is worthwhile to point out that the NAKF-based AR model takes advantage of the gear motion residual signal rather than the TSA signal and thus results in a method superior to previous studies, e.g. [14], in two major aspects. First, the load-dependent feature is strongly

attenuated. Second, fault-induced effects are greatly enhanced. Also, the computational requirements are much lower than those in previous studies, e.g. [4,5,18,20], since it is not necessary to compute either bispectra or time-frequency representations. Moreover, the proposed MRP defined as the outlier percentage of AR model residuals overcomes two natural disadvantages of the kurtosis-based MRK1 and MRK2. First, the MRP is not as sensitive as kurtosis to a few residuals in the tails of the distribution and thus will not show violent fluctuations especially under the healthy state of the gear of interest. Second, the MRP does not show dramatic decreases when multiple gear teeth are involved in the intermediary or advanced faulty state of the gear. Instead, it jumps to and progresses at a sufficiently high level when a fault initiates. In general, the MRP possesses appealing stability in comparison with other recently proposed techniques and thus will not cause false alarms for incipient faults.

The primary concern in the establishment of the AR model is the selection of a proper model order. The predominant objective of order selection in this study is to obtain non-sensitivity of AR model residuals to a variety of possible load conditions in the healthy state of the gear. This should be of no difficulty since the gearbox can always be tested under a number of different load conditions in its running-in period so as to determine a robust order value for future operation. Naturally, the order selected under the consideration of two end load conditions in the healthy state of the gear of interest should also be applicable to load conditions between the tested two boundaries. Any unexpected load level beyond the upper load boundary could be regarded as an abnormality and cause the machine to shut down. A specific and quantitative AR model order selection method is proposed in this study to search for an order value leading to load-independent model fitting.

Finally, we remark that the appealing efficiency of the proposed diagnostic model is gained by the effective combination of gear motion residual signals, AR modeling with a robust order selection and the statistical measure taking the percentage of outliers exceeding the baseline three standard deviation limits. Alternative diagnostic models could be developed by making use of decomposed gear motion signals [1], alternative advanced time series modeling, or more robust statistical measures. To achieve load-independence under varying load conditions, developing a generalized model order selection criterion which is able to summarize in an automated way the seven statistical measures proposed in Section 2.3 could be attempted. In addition, according to the information provided in the original MDTB data CDs, the driven gear was found to be the only faulty component in the gearbox at the end of each test, thus giving no opportunity to explore the performance of the proposed technique when several kinds of faults develop simultaneously, say gear faults plus bearing faults and shaft unbalances. Further research focusing on this issue could be attempted.

Acknowledgements

We are most grateful to the Applied Research Laboratory at Penn State University and the Department of the Navy, Office of the Chief of Naval Research (ONR) for providing the data used to develop this work. We thank Bob Luby at PricewaterhouseCoopers and Murray Wiseman, Dr. Daming Lin and Dr. Dragan Banjevic in the CBM Lab at the University of Toronto for their support. The authors also wish to thank the Natural Sciences and Engineering

Research Council of Canada (NSERC), Material and Manufacturing Ontario of Canada (MMO) and the CBM Consortium members for their financial supports. Finally, we appreciate very much the valuable comments from the referees which greatly helped to improve this work.

References

[1] W.J. Wang, P.D. McFadden, Decomposition of gear motion signals and its application to gearbox diagnostics, *Journal of Vibration and Acoustics* 117 (1995) 363–369.
[2] G. Dalpiaz, A. Rivola, R. Rubini, Effectiveness and sensitivity of vibration processing techniques for local fault detection in gears, *Mechanical Systems and Signal Processing* 14 (2000) 387–412.
[3] W.Q. Wang, F. Ismail, M.F. Golnaraghi, Assessment of gear damage monitoring techniques using vibration measurements, *Mechanical Systems and Signal Processing* 15 (2001) 905–922.
[4] W.J. Wang, P.D. McFadden, Early detection of gear failure by vibration analysis–i. calculation of the time-frequency distribution, *Mechanical Systems and Signal Processing* 7 (1993) 193–203.
[5] W.J. Wang, P.D. McFadden, Early detection of gear failure by vibration analysis–ii. interpretation of the time–frequency distribution using image processing techniques, *Mechanical Systems and Signal Processing* 7 (1993) 205–215.
[6] W.J. Staszewski, K. Worden, G.R. Tomlinson, Time–frequency analysis in gearbox fault detection using the Wigner–Ville distribution and pattern recognition, *Mechanical Systems and Signal Processing* 11 (1997) 673–692.
[7] D. Boulahbal, M. Farid Golnaraghi, F. Ismail, Amplitude and phase wavelet maps for the detection of cracks in geared systems, *Mechanical Systems and Signal Processing* 13 (1999) 423–436.
[8] B. Samanta, Artificial neural networks and genetic algorithms for gear fault detection, *Mechanical Systems and Signal Processing* 18 (2004) 1273–1282.
[9] D. Chen, W.J. Wang, Classification of wavelet map patterns using multi-layer neural networks for gear fault detection, *Mechanical Systems and Signal Processing* 16 (2002) 695–704.
[10] B.A. Paya, I.I. Esat, M.N.M. Badi, Artificial neural network based fault diagnostics of rotating machinery using wavelet transforms as a preprocessor, *Mechanical Systems and Signal Processing* 11 (1997) 751–765.
[11] B.S. Yang, T. Han, J.L. An, ART-KOHONEN neural network for fault diagnosis of rotating machinery, *Mechanical Systems and Signal Processing* 18 (2004) 645–657.
[12] C.K. Mechefske, Objective machinery fault diagnosis using fuzzy logic, *Mechanical Systems and Signal Processing* 12 (1998) 855–862.
[13] G.G. Yen, K.C. Lin, Wavelet packet feature extraction for vibration monitoring, *IEEE Transactions on Industrial Electronics* 47 (3) (2000) 650–667.
[14] W.Y. Wang, A.K. Wong, Autoregressive model-based gear fault diagnosis, *Journal of Vibration and Acoustics* 124 (2002) 172–179.
[15] C.J. Stander, P.S. Heyns, Using vibration monitoring for local fault detection on gears operating under fluctuating load conditions, *Mechanical Systems and Signal Processing* 16 (2002) 1005–1024.
[16] M.M. Roan, J.G. Erling, L.H. Sibul, A new, non-linear, adaptive, blind source separation approach to gear tooth failure detection and analysis, *Mechanical Systems and Signal Processing* 16 (2002) 719–740.
[17] N. Baydar, A. Ball, A comparative study of acoustic and vibration signals in detection of gear failures using Wigner–Ville distribution, *Mechanical Systems and Signal Processing* 15 (2001) 1091–1107.
[18] B.E. Parker Jr., H.A. Ware, D.P. Wipe, W.R. Tompkins, B.R. Clark, E.C. Larson, H.V. Poor, Fault diagnostics using statistical change detection in the bispectral domain, *Mechanical Systems and Signal Processing* 14 (2000) 561–750.
[19] S. Rantala, R. Suoranta, Enhanced vibration monitoring using parametric modelling technique, *IEEE Eighth Instrumentation and Measurement Technology Conference*, 1991, pp. 2–5.
[20] Y.M. Zhan, V. Makis, A.K.S. Jardine, Adaptive model of rotating machinery subject to random deterioration for vibration monitoring, *Journal of Quality in Maintenance Engineering* 9 (2003) 351–375.

[21] MDTB data (Data CDs: TR#5, TR#8, and TR#10), Condition-Based Maintenance Department, Applied Research Laboratory, The Pennsylvania State University, 1998.
[22] C.S. Byington, J.D. Kozlowski, Transitional data for estimation of gearbox remaining useful life, Mechanical Diagnostic Test Bed Data, Applied Research Laboratory, Condition-Based Maintenance Department, The Pennsylvania State University, 2000.
[23] A.J. Miller, A New Wavelet Basis for the Decomposition of Gear Motion Error Signals and its Application to Gearbox Diagnostics, Master of Science Thesis, The Graduate School, The Pennsylvania State University, 1999.